The Journal of Chemical Physics

Revealing the exotic structure of molecules in strong magnetic fields

Cite as: J. Chem. Phys. **156**, 204113 (2022); https://doi.org/10.1063/5.0092520
Submitted: 23 March 2022 • Accepted: 25 April 2022 • Accepted Manuscript Online: 25 April 2022 • Published Online: 25 May 2022

Published open access through an agreement with JISC Collections

Miles J. Pemberton, **Tom J. P. Irons,** **Trygve Helgaker, et al.**

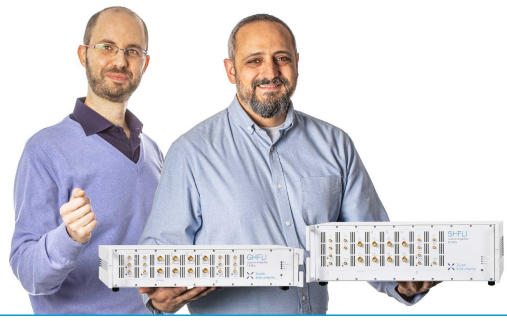

The Journal of Chemical Physics ARTICLE scitation.org/journal/jcp

Revealing the exotic structure of molecules in strong magnetic fields

Cite as: J. Chem. Phys. 156, 204113 (2022); doi: 10.1063/5.0092520
Submitted: 23 March 2022 • Accepted: 25 April 2022 •
Published Online: 25 May 2022

Miles J. Pemberton,[1] Tom J. P. Irons,[1,a)] Trygve Helgaker,[2] and Andrew M. Teale[1,2]

AFFILIATIONS

[1] School of Chemistry, University of Nottingham, Nottingham NG7 2RD, United Kingdom
[2] Hylleraas Centre for Quantum Molecular Sciences, Department of Chemistry, University of Oslo, P.O. Box 1033, Blindern, Oslo N-0315, Norway

[a)] **Author to whom correspondence should be addressed:** tom.irons@nottingham.ac.uk

ABSTRACT

A novel implementation for the calculation of molecular gradients under strong magnetic fields is employed at the current-density functional theory level to optimize the geometries of molecular structures, which change significantly under these conditions. An analog of the *ab initio* random structure search is utilized to determine the ground-state equilibrium geometries for He_n and CH_n systems at high magnetic field strengths, revealing the most stable structures to be those in high-spin states with a planar geometry aligned perpendicular to the field. The electron and current densities for these systems have also been investigated to develop an explanation of chemical bonding in the strong field regime, providing an insight into the exotic chemistry present in these extreme environments.

I. INTRODUCTION

Strong magnetic fields many orders of magnitude larger than those found on Earth are known to exist in the atmospheres of stellar objects, such as magnetic white dwarf stars.[1,2] Under these conditions, interactions with the magnetic field significantly affect the chemistry of molecules, resulting in exotic phenomena, such as the perpendicular paramagnetic bonding mechanism.[3] This can cause significantly different molecular structures to arise in strong fields compared to those at zero field,[4] and in the absence of being able to take direct measurements to interpret astrochemical observations, quantum chemical simulations provide a useful tool to develop an understanding of chemistry under these exotic conditions.

Recently, many quantum chemical methods have been adapted to include a non-perturbative treatment of magnetic field effects on molecular systems, including Hartree–Fock (HF) theory[5,6] and density-functional theory (DFT).[7–10] However, their application has been limited by computational cost, and geometry optimizations under these conditions have only previously been applied to helium clusters and small molecules at the restricted HF level.[11] Recent developments in the QUEST program[12] have enabled the study of larger systems in strong magnetic fields and, for the first time, geometry optimizations of molecules under these conditions can be carried out with an effective treatment of electron correlation at the DFT level.[9,10,13–15]

The present work is concerned with determining the structure of hydrogen-, helium-, and carbon-containing systems (elements present in the atmospheres of magnetic white dwarf stars[2,16–18]) in the presence of strong magnetic fields up to 2.35×10^5 T, where magnetic interactions can be as significant as the Coulomb interactions that dominate on Earth, resulting in exotic molecular structures, which would be impossible to predict from standard chemical intuition. As a consequence, unbiased techniques are needed to search for and elucidate the possible ground-state molecular structures.

II. THEORETICAL BACKGROUND

A. Systems in strong magnetic fields

In atomic units, the non-relativistic electronic Hamiltonian in the presence of a uniform magnetic field $\mathbf{B}$ has the form

$$\hat{\mathcal{H}} = \hat{\mathcal{H}}_0 + \frac{1}{2}(\mathbf{B}\times\mathbf{r}_O)\cdot\hat{\mathbf{p}} + \mathbf{B}\cdot\hat{\mathbf{s}} + \frac{1}{8}(\mathbf{B}\times\mathbf{r}_O)\cdot(\mathbf{B}\times\mathbf{r}_O), \quad (1)$$

where $\hat{\mathcal{H}}_0$ is the electronic Hamiltonian at zero field, $\hat{\mathbf{p}} = -\imath\nabla$ is the canonical momentum operator, $\hat{\mathbf{s}}$ is the spin operator, and $\mathbf{r}_\mathrm{O} = \mathbf{r} - \mathbf{O}$ is the position with respect to an arbitrary gauge origin $\mathbf{O}$. A magnetic field satisfies the relation $\nabla \cdot \mathbf{B} = 0$ and hence can be represented by a vector potential $\mathbf{A}$ for which $\mathbf{B} = \nabla \times \mathbf{A}$. Such a potential is not unique; in the Coulomb gauge, considered in this work, the vector potential is defined such that $\nabla \cdot \mathbf{A} = 0$ everywhere. It follows that for a uniform magnetic field, $\mathbf{A}$ is dependent on the choice of gauge origin $\mathbf{O}$ in the manner

$$\mathbf{A}_\mathrm{O}(\mathbf{r}) = \frac{1}{2}\mathbf{B} \times (\mathbf{r} - \mathbf{O}) \tag{2}$$

with the result that a change in the position of the gauge origin $\mathbf{O} \to \mathbf{O}'$ constitutes a gauge transformation

$$\mathbf{A}_{\mathrm{O}'}(\mathbf{r}) = \mathbf{A}_\mathrm{O}(\mathbf{r}) - \nabla \mathbf{A}_\mathrm{O}(\mathbf{O}') \cdot \mathbf{r} \tag{3}$$

corresponding to the following unitary transformation of the electronic Hamiltonian:

$$\hat{\mathcal{H}}' = \mathrm{e}^{\imath \mathbf{A}_\mathrm{O}(\mathbf{O}')\cdot\mathbf{r}} \hat{\mathcal{H}} \mathrm{e}^{-\imath \mathbf{A}_\mathrm{O}(\mathbf{O}')\cdot\mathbf{r}}. \tag{4}$$

Eigenfunctions Ψ of the Hamiltonian undergo a compensating unitary transformation, $\Psi' = \mathrm{e}^{\imath \mathbf{A}_\mathrm{O}(\mathbf{O}')\cdot\mathbf{r}}\Psi$; the observables of the system, such as the energy and the charge density, therefore, remain invariant to translation of the gauge origin.

The dependence of the wavefunction on the choice of the gauge origin, however, cannot be properly reproduced by a finite basis set expansion of the wavefunction, other than by explicit inclusion of the gauge origin in the basis functions themselves. London atomic orbitals (LAOs) follow this approach, comprising a standard Gaussian-type basis function φ_a with center $\mathbf{R}$ multiplied by a complex phase factor dependent on both the magnetic field and the gauge origin,

$$\omega_a(\mathbf{r}) = \varphi_a(\mathbf{r}) \mathrm{e}^{-\frac{\imath}{2}\mathbf{B}\times(\mathbf{R}-\mathbf{O})\cdot\mathbf{r}}, \tag{5}$$

thereby yielding wavefunctions that exhibit the correct behavior to first order with respect to the magnetic field and observables that are gauge origin invariant.[19–21] Electronic structure calculations in a basis of LAOs permit the effects of applied magnetic fields to be treated non-perturbatively in a gauge-origin invariant manner, allowing the behavior of systems to be studied in magnetic fields of arbitrary strength.[5,9]

This approach to enable electronic structure calculations in strong magnetic fields was first implemented in the LONDON code,[22] being applied to Hartree–Fock,[5] current density-functional,[9] Møller–Plesset perturbation, coupled-cluster,[23] configuration-interaction,[3] and complete-active-space self-consistent field (CASSCF) theories.[3] Several other electronic structure codes have subsequently been developed to include the functionality to consider systems in strong magnetic fields, including BAGEL,[24] CHRONUSQ,[25] and the QUEST program[12] used in this work.

B. Current density functional theory

In the presence of an external magnetic field, given the additional terms containing the field or the associated vector potential in the electronic Hamiltonian, the system can no longer be described exclusively by the charge density as is the case in density functional theory (DFT).[26,27] The complete description of the system may be achieved in one of two ways: by direct inclusion of the magnetic field in the density functional (magnetic field DFT, BDFT)[28,29] or by inclusion of the current density in the density functional (current DFT, CDFT).[7,8,30] A formulation of CDFT applying only to uniform magnetic fields, linear vector potential DFT (LDFT), has been presented in Ref. 31.

In this work, the Vignale–Rasolt formulation of CDFT[7,8] in which the density functional depends on the charge density ρ and the paramagnetic current density $\mathbf{j}_\mathrm{p}$ is utilized. It has been shown[30,32] that a convex-conjugate formulation of CDFT, following Lieb's approach for DFT,[33] may be constructed in this way by re-writing the energy $E(v, \mathbf{A})$, dependent on the scalar potential v and vector potential $\mathbf{A}$, in terms of a modified scalar potential $u = v + \frac{1}{2}\mathbf{A}^2$. The resulting energy functional $\mathcal{E}(u, \mathbf{A})$ is then concave in the potential; the energy functional and its convex-conjugate universal density functional can be written, respectively, as

$$\mathcal{E}(u, \mathbf{A}) = \inf_{\rho, \mathbf{j}_p} \left\{ \mathcal{F}(\rho, \mathbf{j}_\mathrm{p}) + (u|\rho) + (\mathbf{A}|\mathbf{j}_p) \right\}, \tag{6}$$

$$\mathcal{F}(\rho, \mathbf{j}_p) = \sup_{u, \mathbf{A}} \left\{ \mathcal{E}(u, \mathbf{A}) - (u|\rho) - (\mathbf{A}|\mathbf{j}_\mathrm{p}) \right\}, \tag{7}$$

where $(u|\rho) = \int u(\mathbf{r})\rho(\mathbf{r})\mathrm{d}\mathbf{r}$ and $(\mathbf{A}|\mathbf{j}_\mathrm{p}) = \int \mathbf{A}(\mathbf{r}) \cdot \mathbf{j}_p(\mathbf{r})\mathrm{d}\mathbf{r}$ are the potential–density pairings and $\mathcal{F}(\rho, \mathbf{j}_\mathrm{p})$ is the Vignale–Rasolt universal density functional.[7,30]

Applying the Kohn–Sham (KS) decomposition[27] to the Vignale–Rasolt functional, it may be written as[34]

$$\mathcal{F}(\rho, \mathbf{j}_\mathrm{p}) = \mathcal{T}_\mathrm{s}(\rho, \mathbf{j}_\mathrm{p}) + J(\rho) + E_\mathrm{xc}(\rho, \mathbf{j}_\mathrm{p}), \tag{8}$$

where $\mathcal{T}_\mathrm{s}(\rho, \mathbf{j}_p)$ is the non-interacting kinetic energy functional, $J(\rho)$ is the classical Coulomb repulsion energy, and $E_\mathrm{xc}(\rho, \mathbf{j}_\mathrm{p})$ is the exchange–correlation (xc) energy functional. The KS CDFT equations take the form

$$\left[\frac{1}{2}\hat{p}^2 + \frac{1}{2}\{\hat{\mathbf{p}}, \mathbf{A}_\mathrm{s}\} + u_\mathrm{s} + \hat{\mathbf{s}} \cdot (\nabla \times \mathbf{A}_\mathrm{s})\right]\phi_p = \varepsilon_p \phi_p, \tag{9}$$

where ϕ_p and ε_p are the KS orbitals and orbital energies, respectively. In KS CDFT, a non-interacting auxiliary system is introduced with charge density

$$\rho = \sum_\sigma \sum_i^{occ} \phi_{i\sigma}^* \phi_{i\sigma} \tag{10}$$

and paramagnetic current density

$$\mathbf{j}_\mathrm{p} = -\frac{\imath}{2}\sum_\sigma \sum_i^{occ} \left[(\nabla\phi_{i\sigma})\phi_{i\sigma}^* - \phi_{i\sigma}(\nabla\phi_{i\sigma})^*\right] \tag{11}$$

constructed from occupied orbitals with spin σ that reproduce the charge density and paramagnetic current density of the physical system, respectively. The KS potentials $(u_\mathrm{s}, \mathbf{A}_\mathrm{s})$ are given by

$$u_\mathrm{s} = v_\mathrm{ext} + \frac{1}{2}\mathbf{A}_\mathrm{s}^2 + v_\mathrm{J} + v_\mathrm{xc}, \quad \mathbf{A}_\mathrm{s} = \mathbf{A}_\mathrm{ext} + \mathbf{A}_\mathrm{xc} \tag{12}$$

in which v_{ext} and $\mathbf{A}_{ext}$ are the physical external potentials due to the nuclei and magnetic field, respectively, v_J is the Coulomb potential, and v_{xc} and $\mathbf{A}_{xc}$ are the xc scalar and vector potentials, respectively, defined as

$$v_{xc}(\mathbf{r}) = \frac{\delta E_{xc}(\rho, \mathbf{j}_p)}{\delta \rho(\mathbf{r})}, \qquad \mathbf{A}_{xc}(\mathbf{r}) = \frac{\delta E_{xc}(\rho, \mathbf{j}_p)}{\delta \mathbf{j}_p(\mathbf{r})}. \tag{13}$$

Recently, it has been shown that meta-generalized gradient approximation (meta-GGA) functionals provide good accuracy in strong magnetic fields.[10] Most *meta*-GGAs depend on the non-interacting kinetic energy density; in CDFT, this density must be modified to ensure that the exchange–correlation energy remains gauge-origin invariant using, for example, the form suggested by Dobson[35,36] and Becke,[37]

$$\tau_\sigma \to \overline{\tau}_\sigma = \tau_\sigma - \frac{|\mathbf{j}_{p\sigma}|^2}{\rho_\sigma}. \tag{14}$$

In this work, this modification is used in the Tao–Perdew–Staroverov–Scuseria functional, denoted cTPSS,[38,39] previously applied in the context of response theory for weak fields by Bates and Furche[40] and, here, in a non-perturbative manner, allowing its application seamlessly to systems in the presence of weak to strong magnetic fields. In order to describe the effects of correlation on optimized geometries in strong magnetic fields, analytical derivatives as described by Irons *et al.* in Ref. 4 are utilized throughout this work.

C. *Ab initio* random structure search

Molecular structures in a strong magnetic field may be significantly different to those at zero field due to the exotic chemistry in this regime. As a result, choosing appropriate starting structures for geometry optimization is challenging, as it is not necessarily possible to apply simple chemical intuition to start from a structure close to a chemically meaningful energy minimum. Furthermore, a potential energy surface (PES) can contain many minima; the number of minima $n_s(N)$ for an N-atom system was shown by Stillinger[41] to be

$$n_s(N) = e^{\alpha N}, \tag{15}$$

where α is a constant, with this scaling having been observed in computational studies of Lennard-Jones clusters.[42–44] This scaling is likely to be greater in a magnetic field since the energy of each structure will generally no longer be invariant to rotation, resulting in a greater number of local minima in the PES and making the global minimum more difficult to locate.

In order to address these challenges, an analog of the *ab initio* random structure search (AIRSS)[45] has been employed throughout this work. This methodology is typically used for the computational analysis of solid-state structures[46–50] and in the present work is modified to investigate the structure of polyatomic systems in strong magnetic fields.

The approach employed in the present work involves randomly distributing atoms in a shell around a centrally positioned atom, shown on the left in Fig. 1, producing multiple 3D random structures, the geometries of which are optimized and subsequently ranked in order of equilibrium energy to identify the minima of the PES. If sufficient sampling is carried out, then the lowest energy candidate is likely to be the global minimum. In cases where many local minima are accessible, this general approach may struggle to find high symmetry structures (in particular, concerning relative alignment with the magnetic field) from randomly generated 3D starting points. To address this, the approach was augmented such that additional 2D random structures were generated on disks in the plane of and perpendicular to the magnetic field, shown in the center of Fig. 1, while 1D random structures were generated along axes parallel and perpendicular to the magnetic field, shown on the right in Fig. 1. This enabled linear and planar equilibrium structures with a high-symmetry alignment relative to the field to be more easily accessed. The generation of random initial structures with specific symmetries is a feature of the original AIRSS package of Pickard and Needs;[51] for systems larger than those considered in the present work, higher symmetry initial structures could be randomly generated with that approach and rotated to a particular orientation with respect to the magnetic field.

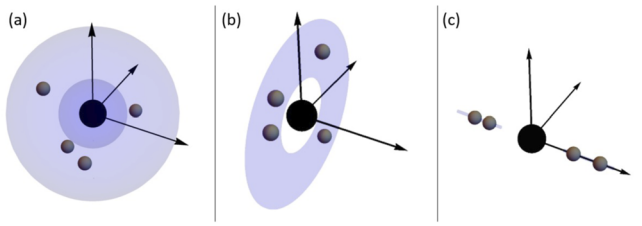

FIG. 1. Distribution of atoms around a centrally positioned atom to produce randomly generated (a) 3D, (b) 2D, and (c) 1D structures for subsequent geometry optimization.

III. RESULTS AND DISCUSSION

A. Computational details

In the following, the structures of He_n and CH_n systems are considered at a range of spin projections (described by their spin quantum numbers M_s) and magnetic field strengths in the range $0–1.0B_0$, where $B_0 = 2.35 \times 10^5$ T is the atomic unit of magnetic field strength. For all calculations, $\mathbf{B}$ is oriented along the z axis.

The AIRSS approach described in Sec. II C was utilized with 32, 48, and 12 randomly generated 3D, 2D, and 1D structures, respectively, each with a minimum distance of 0.5 Å between atoms and between 1.0 and 4.0 Å from the central atom. The structures were first optimized at the HF/aug-cc-pVTZ level and ranked in order of energy to determine which initial structures gave the lowest-energy equilibrium geometry. Only the initial structures of that symmetry were subsequently optimized with cTPSS/aug-cc-pVTZ; this prescreening approach was effective for managing the computational cost. Throughout this work, basis sets are used in their uncontracted form to provide greater flexibility to respond to the effects of the magnetic field.

For all calculations, the optimization method employed was a simple quasi-Newton approach with the Broyden–Fletcher–Goldfarb–Shanno (BFGS) update.[52–55] In all cases, optimization was carried out in Cartesian coordinates.[56–58] This simple choice of coordinate system allows for the effects of the external field to

be incorporated straightforwardly. The convergence criteria suggested by Baker[57] were applied throughout this work: the largest element of the gradient and subsequent step $<3 \times 10^{-4}$ a.u., the root mean square of the gradient and subsequent step $<2 \times 10^{-4}$ a.u., and between iterations the change in energy $<5 \times 10^{-6}$ a.u.

The cTPSS functional was selected for use in this study as it has been shown to yield high accuracy in strong magnetic fields compared with *ab initio* wavefunction methods.[12,59] For both families of systems considered in this work, the calculations were conducted using HF theory and CDFT with cTPSS. Only selected CDFT results are presented here; the full results obtained with CDFT and many obtained with HF theory for comparison can be found in the supplementary material.

To reduce the computational cost, the resolution-of-the-identity (RI) approximation was employed for the two-electron integrals and derivative integrals; recent work utilizing the RI approximation with LAOs has shown that it may be applied in a similar way to its use with GAOs.[4,60,61] This is particularly beneficial due to the large number of calculations required by the AIRSS protocol.

A preliminary study of helium trimers (with $M_s = 0$) at field strengths of $0.4B_0$ and $1.0B_0$ was used to identify a suitable orbital and auxiliary basis set combination. Comparisons were made between conventional (non-RI) calculations, those utilizing the RI auxiliary basis sets of Ref. 62 (designed for calculations in the absence of a magnetic field), and a more conservative one automatically generated using the product space of the orbital basis (AUTOAUX).[63] The results are presented in Table I.

From the energies presented in Table I, it is clear that at both field strengths, RI with the AUTOAUX basis yields energies closer to the non-RI values for a given choice of orbital basis than RI with the optimized-RI auxiliary basis. This result is expected since the AUTOAUX basis is constructed to favor accuracy over efficiency and, thus, contains more functions. Using the aug-cc-pVTZ orbital basis, aug-cc-pVTZ-RI yields energies with mean errors of 76.3 μE_h relative to the non-RI values, compared with mean errors of 5.8 μE_h using the AUTOAUX basis. Furthermore, at $0.4B_0$, the standard RI basis predicts an incorrect energetic ordering of structures A and B; however, the correct ordering is retained using AUTOAUX. Therefore, RI with the aug-cc-pVTZ orbital basis and AUTOAUX auxiliary basis is employed throughout the present work, yielding calculations 5–8 times faster than the non-RI equivalents with negligible loss of accuracy.

B. Helium clusters in strong magnetic fields

At zero field, the ground-state of the helium atom has $M_s = 0$ with electronic configuration $1s^{\alpha\beta}$, while at a field strength of $1.0B_0$, the ground-state becomes that with $M_s = -1$ and electronic configuration $1s^{\beta}2p^{\beta}_{-1}$ because of spin and orbital Zeeman interactions in Eq. (1), which stabilize the $M_s = -1$ triplet component and $2p_{-1}$ orbital, respectively, in a magnetic field.

Using the AIRSS approach, geometries of the helium structures were generated and subsequently optimized as outlined in Sec. III A. The cTPSS results are discussed here; the HF results for both He_n and CH_n (discussed in Sec. III C) are presented in Secs. V and VI of the supplementary material. While qualitatively similar to the cTPSS results, their energies do not include any contribution from electron correlation.

In many cases, particularly at lower field strengths, the structures are only weakly bound and energy differences between optimized structures are relatively small. Here, the procedural modifications to the random structure generation described in Sec. II C were essential for accessing the minimum energy geometries. The large number of solutions accessible for He_5 can be seen in Fig. 2, where for each M_s value, the lowest energy solution at each field strength falls on the convex hull of all calculated energies of that spin projection. Figure 2 demonstrates that structures with negative M_s values decrease in energy due, at least in part, to the spin-Zeeman effect, while the diamagnetic $M_s = 0$ systems increase in energy with increasing field strength. The ground state at $1.0B_0$ has the most negative possible M_s value and adopts a planar structure perpendicular to the field. The ground-state equilibrium geometries at each field strength are shown in Fig. 3.

As the field strength increases from 0 to $1.0B_0$, there is an increase in the dissociation energies of the He_5 structures. The different fragmentation pathways of the He_5 systems have been established from geometry optimizations carried out on smaller He_n clusters, where all of the possible dissociation products and their energies (shown in Secs. I and III of the supplementary material) were considered. The lowest energy dissociation pathway for the

TABLE I. Convergence of the energy of the helium trimer (with $M_s = 0$) as a function of magnetic field strength for optimizations computed using HF theory from two randomly generated AIRSS candidate structures ("A" and "B"). Magnetic fields of $0.4B_0$ and $1.0B_0$ along the *z* axis were considered. Two standard orbital basis sets aug-cc-pVDZ[64–66] and aug-cc-pVTZ[64,65] are presented. Results with standard RI basis sets[62] (-RI suffix) are compared with those using the AUTOAUX basis and without the RI approximation.

		$\lvert\mathbf{B}\rvert = 0.4B_0$		$\lvert\mathbf{B}\rvert = 1.0B_0$	
Orbital basis	Auxiliary basis	E_A/E_h	E_B/E_h	E_A/E_h	E_B/E_h
aug-cc-pVDZ	aug-cc-pVDZ-RI	−8.474 893	−8.474 926	−8.027 307	−8.009 060
	AUTOAUX	−8.473 639	−8.473 691	−8.025 935	−8.008 540
	Non-RI	−8.473 640	−8.473 693	−8.025 937	−8.008 668
aug-cc-pVTZ	aug-cc-pVTZ-RI	−8.491 217	−8.491 221	−8.061 435	−8.041 717
	AUTOAUX	−8.491 142	−8.491 138	−8.061 345	−8.041 759
	Non-RI	−8.491 144	−8.491 138	−8.061 347	−8.041 778

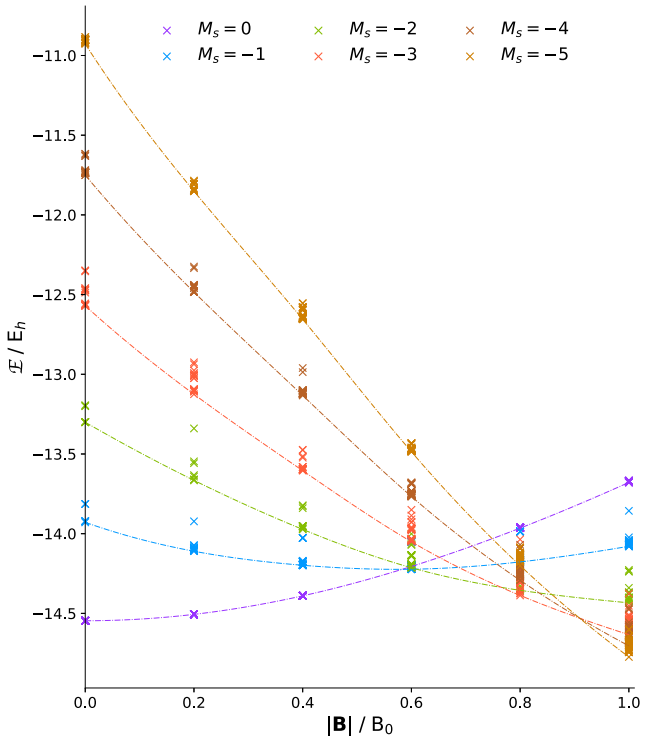

FIG. 2. A convex hull plot for He_5 showing the optimized energies obtained from random initial structures of He_5 with $M_s = 0, -1, -2, -3, -4, -5$ with $|\mathbf{B}| = 0.0–1.0B_0$ at intervals of $0.2B_0$. The lowest energy structures of each spin projection from $|\mathbf{B}| = 0.0–1.0B_0$ fall on the convex hull, shown by the dashed dotted lines.

ground-state He_5 clusters at each field strength is given in Table II in which the notation $He_n^{(M_s)}$ is used. In all cases, He_5 dissociates into two fragments, each of which are in their ground-states.

The ground-state structures at $|\mathbf{B}| = 0$ and $|\mathbf{B}| = 0.2B_0$ are 3D $He_5^{(0)}$ clusters with C_1 symmetry and, in the case of the $|\mathbf{B}| = 0.2B_0$ structure, with no particular alignment to the field. An increase in the field strength to $|\mathbf{B}| = 0.4B_0$ causes the $He_5^{(0)}$ ground-state structure to align in a plane perpendicular to the direction of the applied field as a result of the stronger magnetic interactions. In all of these $M_s = 0$ cases, the lowest energy dissociation involves the removal of a single helium atom.

At $|\mathbf{B}| = 0.6B_0$ with ground-state $He_5^{(-1)}$, the lowest energy dissociation involves the loss of a $He^{(0)}$ atom to form $He_4^{(-1)}$, which further dissociates through the loss of a second $He^{(0)}$ atom, resulting in the clearly identifiable linear $He_3^{(-1)}$ subsystem that can be seen in Fig. 3 and is aligned parallel to the field.

Moving to $|\mathbf{B}| = 0.8B_0$, $He_5^{(-3)}$ becomes the ground-state system, containing two distinct $He_2^{(-1)}$ subsystems aligned parallel to the field. These dimers are remarkably stable in a strong magnetic field, having been investigated in detail by Austad *et al.*[67] and demonstrated by the dissociation energies for this structure given in Table I(c) of the supplementary material. The stability of this $He_2^{(-1)}$ dimer rationalizes the dissociation of $He_5^{(-3)}$ into a $He_2^{(-1)}$ dimer and the $He_3^{(-2)}$ system.

At a magnetic field strength of $|\mathbf{B}| = 1.0B_0$, $He_5^{(-5)}$ is the ground-state system and has the highest dissociation energy of any of the ground-state systems, suggesting that systems can become more strongly bound at higher field strengths. The shape of the $He_5^{(-5)}$ cluster at $|\mathbf{B}| = 1.0B_0$ is very similar to the shape of $He_5^{(0)}$ at the same field strength; however, the more negative spin-projection system is much more strongly bound with a dissociation energy around ten times greater than that of the closed-shell system. This builds on the work by Tellgren *et al.*[11] in which restricted HF theory was used and higher spin states could not be accessed, but which found that the closed shell He_5 cluster was planar perpendicular to the field and very weakly bound. Furthermore, the dissociation energy calculated using DFT with the cTPSS functional is around 10% higher than the same value calculated using HF theory, indicating the importance of considering correlation effects in these studies. The importance of electron correlation in paramagnetically bound helium clusters was noted by Stopkowicz *et al.*,[23] who compared the binding energy of He_3 calculated using HF theory and coupled-cluster singles–doubles–perturbative-triples [CCSD(T)] theory.

The current density induced by an external magnetic field has been extensively used in explaining the electronic structure in a magnetic field.[68–71] The stability of the $He_5^{(-5)}$ clusters at high field

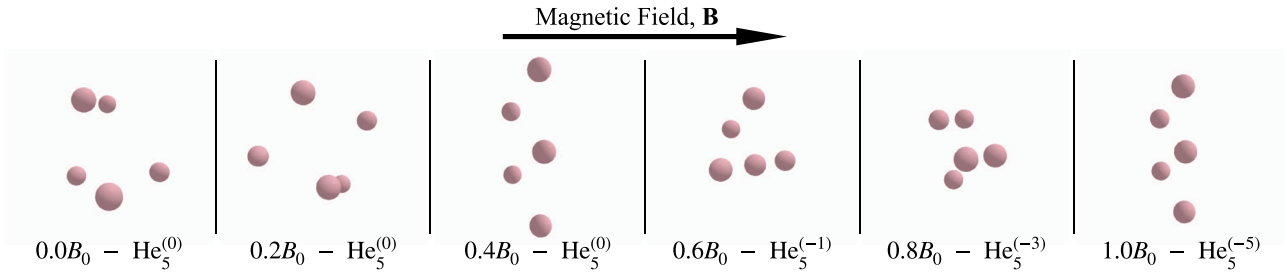

FIG. 3. Ground-state structures for He_5 at $|\mathbf{B}| = 0.0–1.0B_0$ in increments of $0.2B_0$ with the direction of the magnetic field relative to the molecular plane indicated by the arrow.

TABLE II. Lowest energy dissociation pathways and their associated energies for the ground-state He_5 structures at $|\mathbf{B}| = 0.0–1.0B_0$ in increments of $0.2B_0$, calculated from the energies of the He_5 clusters and the relevant smaller He_n fragments obtained from the AIRSS analysis for these systems. The notation $He_n^{(M_s)}$ is used here.

$\lvert\mathbf{B}\rvert/B_0$	Ground state	E/E_h	Lowest energy dissociation	ΔE (kJ mol^{-1})
0.0	$He_5^{(0)}$	−14.546 161	$He_5^{(0)} \rightarrow He_4^{(0)} + He^{(0)}$	0.34
0.2	$He_5^{(0)}$	−14.506 096	$He_5^{(0)} \rightarrow He_4^{(0)} + He^{(0)}$	0.42
0.4	$He_5^{(0)}$	−14.389 737	$He_5^{(0)} \rightarrow He_4^{(0)} + He^{(0)}$	1.23
0.6	$He_5^{(-1)}$	−14.222 990	$He_5^{(-1)} \rightarrow He_4^{(-1)} + He^{(0)}$	8.84
0.8	$He_5^{(-3)}$	−14.387 322	$He_5^{(-3)} \rightarrow He_3^{(-2)} + He_2^{(-1)}$	73.35
1.0	$He_5^{(-5)}$	−14.773 498	$He_5^{(-5)} \rightarrow He_4^{(-4)} + He^{(-1)}$	136.03

strengths can be rationalized by considering the charge and current densities of the equilibrium geometry relative to those of the isolated atoms, plotted for $He_5^{(0)}$ and $He_5^{(-5)}$ at $|\mathbf{B}| = 1.0B_0$ in the upper and lower panels of Fig. 4, respectively. It can be seen that in $He_5^{(-5)}$, there is an accumulation of charge in the interatomic regions; the local paratropic current flow indicates that this is caused by the magnetic field rather than conventional bonding, thus stabilizing the structure. In contrast, there is very little build-up of electron density and no strong current between the atoms in $He_5^{(0)}$, hence the weakly bound nature of this low spin system.

C. CH_n systems in strong magnetic fields

The AIRSS approach was also applied to CH_n with $1 \le n \le 4$. An initial study was conducted following the same approach as for He_n. However, in some cases, it was observed that the lowest-energy structures with a given M_s at a particular field strength had energies above the convex hull formed from the energies of the lowest-energy structures with that M_s at the other field strengths. This was particularly the case at low field strengths and indicated that the ground-state equilibrium geometry had not been located. Further sampling of initial structures with smaller internuclear distances yielded lower energy solutions, which fell on the convex hulls formed by the lowest-energy structures for the given M_s at the other field strengths, as shown in Fig. 5 for CH_4. This highlights two important aspects of the AIRSS approach— namely, that the volume for sampling atomic positions must be chosen carefully and that the convex hull analysis can help identify where additional sampling is required to obtain the ground state.

The general trends observed for CH_n closely follow those observed with the helium clusters, where systems with more negative spin projection become increasingly stabilized at higher field strengths due to the spin-Zeeman effect. The $CH_4^{(-4)}$ system becomes the ground-state at higher field strengths, as presented in the convex hull plot for this combination of atoms in Fig. 5. For the CH_4 system, the point at which the ground state switches to more negative M_s occurs at a lower field strength and over a smaller field range than it does for the He_5 cluster. This happens since the energy of the carbon atom becomes stabilized more quickly by the magnetic field as a result of the occupation of the high angular momentum $3d_{-2}$ orbital, which is lowered in energy at high field strengths by the

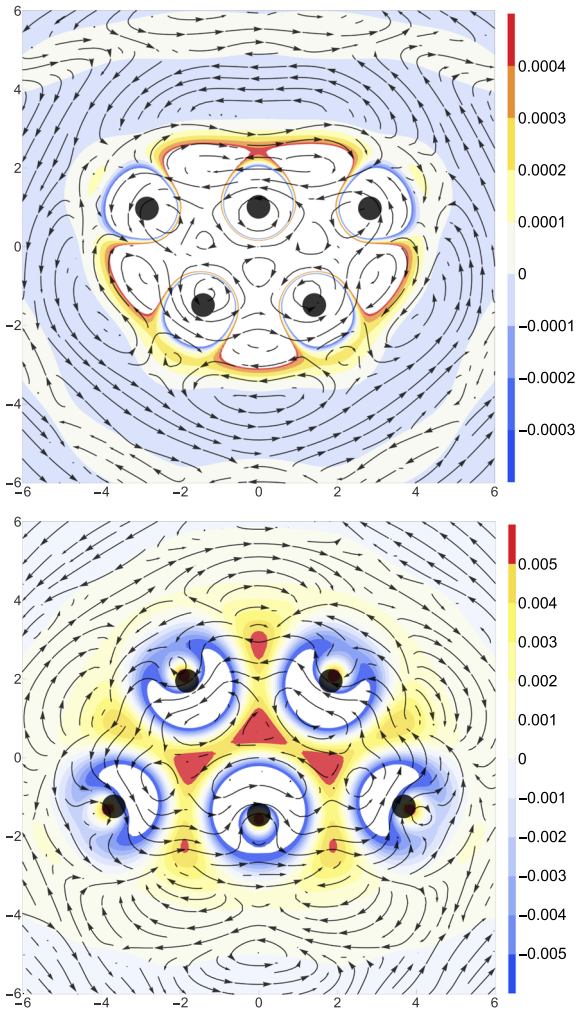

FIG. 4. Charge density (contours) and current density (streamlines) plots for two He_5 systems at $M_s = 0$ (upper) and $M_s = -5$ (lower) compared to the respective charge and current densities of the isolated atoms, considered in a magnetic field of strength $1.0B_0$ aligned perpendicular to the plane of the atoms. The plots are shown in the xy plane intersecting the atomic positions with the magnetic field directed in the z-direction out of the plane.

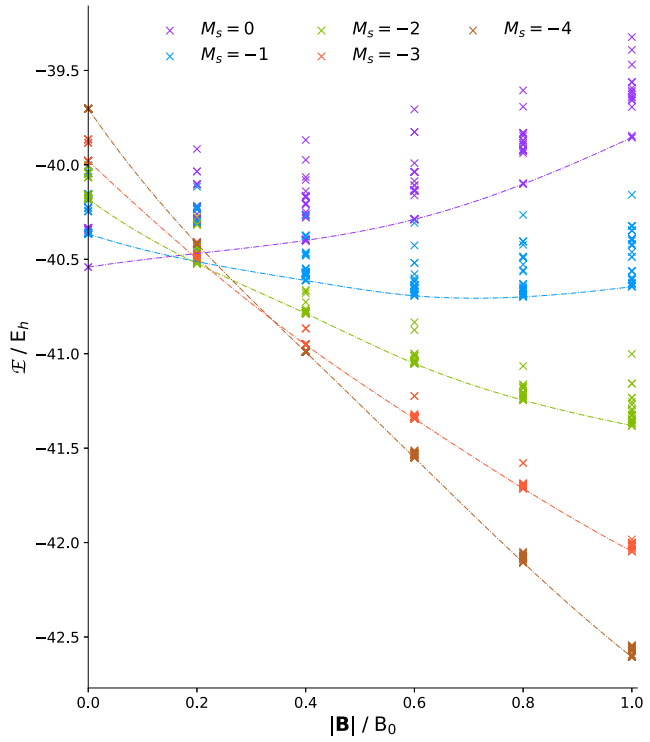

FIG. 5. A convex hull plot for CH_4 showing the optimized energies obtained from random initial structures of CH_4 with $M_s = 0, -1, -2, -3, -4$ with $|\mathbf{B}| = 0.0–1.0B_0$ at intervals of $0.2B_0$. The lowest energy structures of each spin-projection from $|\mathbf{B}| = 0.0–1.0B_0$ form a convex hull, shown by the dashed dotted lines.

orbital paramagnetic terms in the molecular Hamiltonian in Eq. (1). Indeed, the energy difference between the highest occupied α orbital and the lowest unoccupied β orbital is lower in CH_4 at zero field than in He_5 and closes more rapidly with field strength; thus, the first $\alpha \rightarrow \beta$ transition becomes energetically favorable at a lower field strength.

Overall, the CH_4 system moves from a tetrahedral $CH_4^{(0)}$ molecule at zero field to a planar $CH_4^{(-4)}$ molecule at higher field strengths. However, the stability of the covalently bound $CH_4^{(0)}$ molecule at zero field introduces some differences in the behavior of the dissociation energies between the CH_n and He_n systems, which are given along with the respective energies for the ground-state systems at different field strengths in Table III. The corresponding structures are illustrated in Fig. 6.

It is apparent that the most strongly bound structure with respect to dissociation is the tetrahedral $CH_4^{(0)}$ molecule due to the covalent bonding between the carbon and hydrogen atoms. However, the presence of an external magnetic field destabilizes the diamagnetic $CH_4^{(0)}$ system with respect to its dissociation products (these dissociation energies along with convex hull plots for these species are given in Secs. II and IV of the supplementary material), whereas the stability of the systems with $M_s < 0$ increases with field strength. This causes the covalent bonds to break, and the more negative spin-projection ground-states adopt new conformations in a plane perpendicular to the field.

At $|\mathbf{B}| = 0.2B_0$, the $CH_4^{(-2)}$ system is the ground state. The lowest energy dissociation pathway in this case is the removal of a single weakly bound hydrogen atom, present at a considerable distance from the rest of the $CH_4^{(-2)}$ system, as can be seen in Fig. 6. Above this field strength, the $M_s = -4$ system becomes the ground-state.

The geometries of $CH_4^{(-4)}$ systems at $|\mathbf{B}| = 0.4B_0$, $0.6B_0$, and $0.8B_0$ are planar and perpendicular to the field. However, this planar configuration is lost at $|\mathbf{B}| = 1.0B_0$ with the C–H bonds no longer being exactly perpendicular to the magnetic field. This is due to electrostatic repulsion between the constituent atoms, rationalized by considering the mean C–H and H–H internuclear distances for different high-field $CH_4^{(-4)}$ systems, shown in Table IV. The C–H and H–H internuclear distances both decrease with increasing field strength as a result of favorable magnetic interactions between hydrogen atoms as described in Ref. 3. However, as the atoms approach each other more closely, electrostatic repulsion becomes increasingly significant; the most energetically favorable arrangement of these atoms ceases to be a planar configuration but instead is the one in which the carbon atom becomes displaced from the plane in order to preserve the more stabilizing paramagnetic interactions between adjacent hydrogen atoms.

The bonding in these systems is analyzed through the use of current density plots in Fig. 7 (analogous to those for He_5 in Fig. 4)

TABLE III. Lowest energy dissociation pathways and their associated energies for the ground-state CH_4 structures at $|\mathbf{B}| = 0.0–1.0B_0$ in increments of $0.2B_0$, calculated from the energies of the CH_4 clusters and the relevant smaller CH_n and H_n fragments obtained from the AIRSS analysis for these systems. The notation $CH_n^{(M_s)}$ is used here.

$\lvert\mathbf{B}\rvert/B_0$	Ground state	E/E_h	Lowest energy dissociation	ΔE (kJ mol^{-1})
0.0	$CH_4^{(0)}$	−40.541 554	$CH_4^{(0)} \rightarrow CH_2^{(0)} + H_2^{(0)}$	546.71
0.2	$CH_4^{(-2)}$	−40.522 488	$CH_4^{(-2)} \rightarrow CH_3^{(-3/2)} + H^{(-1/2)}$	0.34
0.4	$CH_4^{(-4)}$	−40.991 056	$CH_4^{(-4)} \rightarrow CH_3^{(-7/2)} + H^{(-1/2)}$	5.23
0.6	$CH_4^{(-4)}$	−41.550 562	$CH_4^{(-4)} \rightarrow CH_3^{(-7/2)} + H^{(-1/2)}$	31.95
0.8	$CH_4^{(-4)}$	−42.105 474	$CH_4^{(-4)} \rightarrow CH_3^{(-7/2)} + H^{(-1/2)}$	41.94
1.0	$CH_4^{(-4)}$	−42.605 768	$CH_4^{(-4)} \rightarrow CH_3^{(-7/2)} + H^{(-1/2)}$	49.29

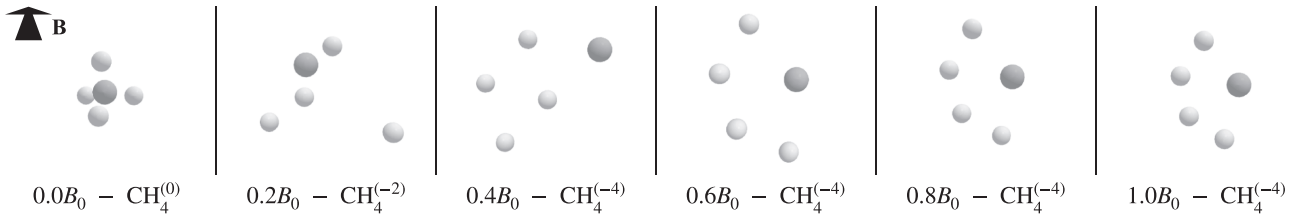

FIG. 6. Ground-state structures for CH_4 at $|\mathbf{B}| = 0.0$–$1.0B_0$ in increments of $0.2B_0$ with the direction of the magnetic field relative to the molecular plane indicated by the arrow (pointing into the plane of the image).

TABLE IV. Mean internuclear C–H and H–H distances in the $CH_4^{(-4)}$ structure at three magnetic field strengths.

$\|\mathbf{B}\|/B_0$	Mean C–H distance (Å)	Mean H–H distance (Å)
0.6	2.46	1.87
0.8	2.14	1.59
1.0	1.95	1.41

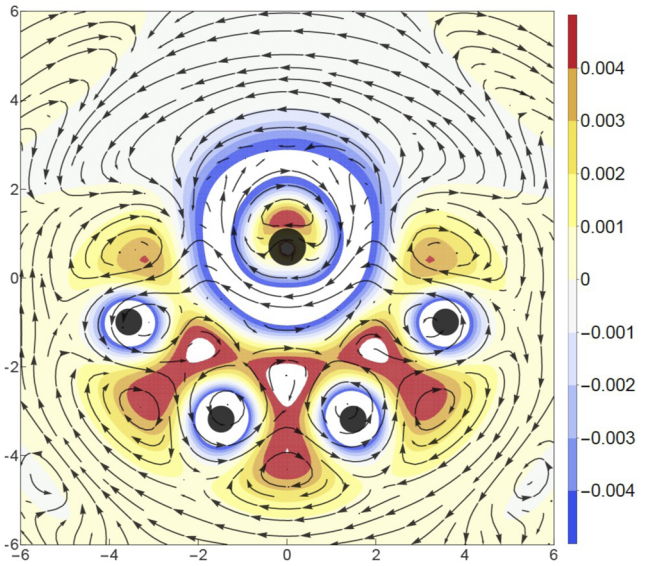

FIG. 7. Electron density (contours) and current density (streamlines) plots for the CH_4 system with $M_s = -4$ compared to the respective electron and current densities of the isolated atoms, considered in a magnetic field of strength $0.8B_0$ aligned perpendicular to the plane of the atoms. The plots are shown in the xy plane intersecting the atomic positions with the magnetic field directed in the z-direction out of the plane.

for the $CH_4^{(-4)}$ system at $|\mathbf{B}| = 0.8B_0$. The build-up of the electron density between the hydrogen atoms confirms the presence of the paramagnetic bonding regime, which is further supported by the clockwise paratropic current density streamlines.

IV. CONCLUSION

In this work, the structures of He_n clusters and CH_n systems in strong magnetic fields have been investigated using a novel implementation for the evaluation of molecular gradients at the HF and CDFT levels of theory in a basis of London atomic orbitals.[4] Since the strong magnetic fields can lead to exotic chemical behavior, a modification of the AIRSS method[45] was employed to optimize randomly generated structures and locate the ground-state for these systems. This modification can be applied in future studies on other small molecules under similar extreme conditions.

As high-spin states are increasingly favored over low-spin states in a magnetic field of increasing field strength, we observe the usual reordering of electronic states driven primarily by the linear spin-Zeeman effect lowering the energy of high-spin states and the quadratic diamagnetic effect raising the energy of the lower-spin states with increasing field strength, as previously observed for atoms—see, for example, Refs. 23 and 67. Remarkably, this convex behavior is only observed if the geometrical structure of the system is fully optimized at each field strength. As the spin-Zeeman interaction breaks covalent bonds by promoting alpha electrons to beta electrons, the system becomes stabilized by the perpendicular paramagnetic bonding mechanism,[3] assuming a (near-)planar configuration perpendicular to the field to maximize the effect of paramagnetic bonding. At the highest field strengths considered, the confining effects of the external field cause the inter-atomic distances to shorten in $CH_4^{(-4)}$, and this leads to distortion away from a planar structure as Coulomb interactions again become more significant and have to be counterbalanced with the confinement due to the field. This case exemplifies how the Coulomb interactions and those with the external field interplay—leading to an exotic chemistry under these conditions.

The current densities induced by the field were used to rationalize the bonding in He_5 and CH_4, revealing that paratropic current densities in the interatomic regions cause an accumulation of β-charge density, indicative of chemical bonding occurring due to the external magnetic field and thus explaining why these high-spin structures become more strongly bound at higher field strengths.

The predictions of molecular structures in strong magnetic fields obtained with this approach could facilitate new insights into the environments on the surface of magnetic white dwarf stars by aiding in the interpretation of astrochemical spectra from these bodies as computational modeling has previously led to the identification of C–C and C–H bonds in these environments,[72,73] and due to the chemical composition of magnetic white dwarf stars, He and

CH_n clusters are likely candidates for any further molecules to be identified.

SUPPLEMENTARY MATERIAL

See the supplementary material for convex hull plots and tables of dissociation energies for He_5 and CH_4 computed with HF along with the convex hull plots and tables of dissociation energies for their possible dissociation fragments computed with HF and CDFT.

ACKNOWLEDGMENTS

We acknowledge financial support from the European Research Council under H2020/ERC Consolidator Grant top DFT (Grant No. 772259). This work was partially supported by the Research Council of Norway through its Centres of Excellence scheme (Project No. 262695). We are grateful for access to the University of Nottingham's Augusta HPC service. The authors are grateful to Professor D. Sundholm and Dr. M. Dimitrova for insightful discussions on the structure of molecular species in strong magnetic fields.

AUTHOR DECLARATIONS

Conflict of Interest

The authors have no conflicts to disclose.

DATA AVAILABILITY

The data that support the findings of this study are available within the article and its supplementary material.

REFERENCES

[1] R. H. Garstang, Rep. Prog. Phys. **40**, 105 (1977).
[2] J. R. P. Angel, Astrophys. J. **216**, 1 (1977).
[3] K. K. Lange, E. I. Tellgren, M. R. Hoffmann, and T. Helgaker, Science **337**, 327 (2012).
[4] T. J. P. Irons, G. David, and A. M. Teale, J. Chem. Theory Comput. **17**, 2166 (2021).
[5] E. I. Tellgren, A. Soncini, and T. Helgaker, J. Chem. Phys. **129**, 154114 (2008).
[6] E. I. Tellgren, T. Helgaker, and A. Soncini, Phys. Chem. Chem. Phys. **11**, 5489 (2009).
[7] G. Vignale and M. Rasolt, Phys. Rev. Lett. **59**, 2360 (1987).
[8] G. Vignale and M. Rasolt, Phys. Rev. B **37**, 10685 (1988).
[9] E. I. Tellgren, A. M. Teale, J. W. Furness, K. K. Lange, U. Ekström, and T. Helgaker, J. Chem. Phys. **140**, 034101 (2014).
[10] J. W. Furness, J. Verbeke, E. I. Tellgren, S. Stopkowicz, U. Ekström, T. Helgaker, and A. M. Teale, J. Chem. Theory Comput. **11**, 4169 (2015).
[11] E. I. Tellgren, S. S. Reine, and T. Helgaker, Phys. Chem. Chem. Phys. **14**, 9492 (2012).
[12] QUEST, a rapid development platform for quantum electronic structure techniques, quest.codes, 2017.
[13] T. J. P. Irons, J. W. Furness, M. S. Ryley, J. Zemen, T. Helgaker, and A. M. Teale, J. Chem. Phys. **147**, 134107 (2017).
[14] T. J. P. Irons, L. Spence, G. David, B. T. Speake, T. Helgaker, and A. M. Teale, J. Phys. Chem. A **124**, 1321 (2020).
[15] M. Wibowo, T. J. P. Irons, and A. M. Teale, J. Chem. Theory Comput. **17**, 2137 (2021).
[16] G. D. Schmidt, J. Liebert, H. C. Harris, C. C. Dahn, and S. K. Leggett, Astrophys. J. **512**, 916 (1999).
[17] T. Vornanen, S. V. Berdyugina, A. V. Berdyugin, and V. Piirola, Astrophys. J. **720**, L52 (2010).
[18] P. Dufour, J. Liebert, G. Fontaine, and N. Behara, Nature **450**, 522 (2007).
[19] F. London, J. Phys. Radium **8**, 397 (1937).
[20] R. Ditchfield, Mol. Phys. **27**, 789 (1974).
[21] R. Ditchfield, J. Chem. Phys. **65**, 3123 (1976).
[22] LONDON, a quantum chemistry program for plane–wave/GTO hybrid basis sets and finite magnetic field calculations, londonprogram.org.
[23] S. Stopkowicz, J. Gauss, K. K. Lange, E. I. Tellgren, and T. Helgaker, J. Chem. Phys. **143**, 074110 (2015).
[24] BAGEL, brilliantly advanced general electronic-structure library, nubakery.org, published under the GNU General Public License.
[25] D. B. Williams-Young, A. Petrone, S. Sun, T. F. Stetina, P. Lestrange, C. E. Hoyer, D. R. Nascimento, L. Koulias, A. Wildman, J. Kasper, J. J. Goings, F. Ding, A. E. DePrince, E. F. Valeev, and X. Li, Wiley Interdiscip. Rev.: Comput. Mol. Sci. **10**, e1436 (2019).
[26] P. Hohenberg and W. Kohn, Phys. Rev. **136**, B864 (1964).
[27] W. Kohn and L. J. Sham, Phys. Rev. **140**, A1133 (1965).
[28] C. J. Grayce and R. A. Harris, Phys. Rev. A **50**, 3089 (1994).
[29] F. R. Salsbury and R. A. Harris, J. Chem. Phys. **107**, 7350 (1997).
[30] E. I. Tellgren, S. Kvaal, E. Sagvolden, U. Ekström, A. M. Teale, and T. Helgaker, Phys. Rev. A **86**, 062506 (2012).
[31] E. I. Tellgren, A. Laestadius, T. Helgaker, S. Kvaal, and A. M. Teale, J. Chem. Phys. **148**, 024101 (2018).
[32] S. Kvaal, A. Laestadius, E. Tellgren, and T. Helgaker, J. Phys. Chem. Lett. **12**, 1421 (2021).
[33] E. H. Lieb, Int. J. Quantum Chem. **24**, 243 (1983).
[34] S. Reimann, A. Borgoo, J. Austad, E. I. Tellgren, A. M. Teale, T. Helgaker, and S. Stopkowicz, Mol. Phys. **117**, 97 (2018).
[35] J. F. Dobson, J. Phys.: Condens. Matter **4**, 7877 (1992).
[36] J. F. Dobson, J. Chem. Phys. **98**, 8870 (1993).
[37] A. D. Becke, Can. J. Chem. **74**, 995 (1996).
[38] J. Tao, J. P. Perdew, V. N. Staroverov, and G. E. Scuseria, Phys. Rev. Lett. **91**, 146401 (2003).
[39] J. Tao, Phys. Rev. B **71**, 205107 (2005).
[40] J. E. Bates and F. Furche, J. Chem. Phys. **137**, 164105 (2012).
[41] F. H. Stillinger, Phys. Rev. E **59**, 48 (1999).
[42] M. R. Hoare and J. McInnes, Faraday Discuss. Chem. Soc. **61**, 12 (1976).
[43] C. J. Tsai and K. D. Jordan, J. Phys. Chem. **97**, 11227 (1993).
[44] J. P. K. Doye, M. A. Miller, and D. J. Wales, J. Chem. Phys. **111**, 8417 (1999).
[45] C. J. Pickard and R. J. Needs, J. Phys.: Condens. Matter **23**, 053201 (2011).
[46] C. J. Pickard and R. J. Needs, Phys. Rev. Lett. **97**, 045504 (2006).
[47] C. J. Pickard and R. J. Needs, Nat. Phys. **3**, 473 (2007).
[48] C. J. Pickard and R. J. Needs, Phys. Status Solidi B **246**, 536 (2009).
[49] C. J. Pickard and R. J. Needs, J. Chem. Phys. **127**, 244503 (2007).
[50] C. J. Pickard and R. J. Needs, J. Phys.: Condens. Matter **21**, 452205 (2009).
[51] The AIRSS Package, airss-docs.github.io, 2022.
[52] C. G. Broyden, IMA J. Appl. Math. **6**, 76 (1970).
[53] R. Fletcher, Comput. J. **13**, 317 (1970).
[54] D. Goldfarb, Math. Comput. **24**, 23 (1970).
[55] D. F. Shanno, Math. Comput. **24**, 647 (1970).
[56] J. Baker, J. Comput. Chem. **13**, 240 (1992).
[57] J. Baker, J. Comput. Chem. **14**, 1085 (1993).
[58] J. Baker and D. Bergeron, J. Comput. Chem. **14**, 1339 (1993).
[59] S. Sen and E. I. Tellgren, J. Chem. Theory Comput. **17**, 1480 (2021).
[60] A. Pausch and W. Klopper, Mol. Phys. **118**, e1736675 (2020).
[61] G. David, T. J. P. Irons, A. E. A. Fouda, J. W. Furness, and A. M. Teale, J. Chem. Theory Comput. **17**, 5492 (2021).
[62] F. Weigend, A. Köhn, and C. Hättig, J. Chem. Phys. **116**, 3175 (2002).

[63]G. L. Stoychev, A. A. Auer, and F. Neese, J. Chem. Theory Comput. **13**, 554 (2017).
[64]R. A. Kendall, T. H. Dunning, and R. J. Harrison, J. Chem. Phys. **96**, 6796 (1992).
[65]D. E. Woon and T. H. Dunning, J. Chem. Phys. **98**, 1358 (1993).
[66]T. H. Dunning, J. Chem. Phys. **90**, 1007 (1989).
[67]J. Austad, A. Borgoo, E. I. Tellgren, and T. Helgaker, Phys. Chem. Chem. Phys. **22**, 23502 (2020).
[68]R. D. Reynolds and T. Shiozaki, Phys. Chem. Chem. Phys. **17**, 14280 (2015).
[69]H. Fliegl, S. Taubert, O. Lehtonen, and D. Sundholm, Phys. Chem. Chem. Phys. **13**, 20500 (2011).
[70]D. Sundholm, H. Fliegl, and R. J. F. Berger, Wiley Interdiscip. Rev.: Comput. Mol. Sci. **6**, 639 (2016).
[71]I. Benkyi and D. Sundholm, J. Phys. Chem. A **123**, 284 (2018).
[72]J. R. P. Angel and J. D. Landstreet, Astrophys. J. **191**, 457 (1974).
[73]S. V. Berdyugina, A. V. Berdyugin, and V. Piirola, Phys. Rev. Lett. **99**, 091101 (2007).